POLISH MARITIME RESEARCH 3 (123) 2024 Vol. 31; pp. 85-93
10.2478/pomr-2024-0038

Fault Diagnosis of Marine Diesel Engine Based on Multi-scale Time Domain Decomposition and Convolutional Neural Network

Congyue Li
Marine Engineering College, Dalian Maritime University, Dalian, China
Dexin Cui*
NINGBO OCEAN SHIPPING CO.,LTD, Ningbo, China

* Corresponding author: *cuidexin2008@126.com (Dexin Cui)*

ABSTRACT

Marine diesel engines work in an environment with multiple excitation sources. Effective feature extraction and fault diagnosis of diesel engine vibration signals have become a hot research topic. Time-domain synchronous averaging (TSA) can effectively handle vibration signals. However, the key phase signal required for TSA is difficult to obtain. During signal processing, it can result in the loss of information on fault features. In addition, frequency multiplication signal waveforms are mixed. To address this problem, a multi-scale time-domain averaging decomposition (MTAD) method is proposed and combined with signal-to-image conversion and a convolutional neural network (CNN), to perform fault diagnosis on a marine diesel engine. Firstly, the vibration signals are decomposed by MTAD. The MTAD method does not require the acquisition of the key phase signal and can effectively overcome signal aliasing. Secondly, the decomposed signal components are converted into 2-D images by signal-to-image conversion. Finally, the 2-D images are input into the CNN for adaptive feature extraction and fault diagnosis. Through experiments, it is verified that the proposed method has certain noise immunity and superiority in marine diesel engine fault diagnosis.

Keywords: multi-scale time-domain averaging decomposition; signal-to-conversion; CNN; marine diesel engine; fault diagnosis

INTRODUCTION

The diesel engine is the heart of the cabin. It operates in an environment with multiple excitation sources and its vibration signals are characterised by non-linearity and non-stationarity [1]. Research into fault diagnosis is very important, to reduce downtime and improve navigation safety.

In recent years, relevant scholars have analysed vibration signals from the time-frequency domain perspective. The main methods include short-time Fourier transform (STFT) [2], wavelet transforms (WT) [3-5], Hilbert Huang transforms (HHT) [6], and variational mode decomposition (VMD) [7]. Although the above methods are very widely used, they also have certain drawbacks. For example, the window function of the STFT is fixed and is not suitable for the analysis of non-stationary signals [8]. WT needs to manually select the basis function, and different basis functions will affect the diagnosis results [9]. HHT has difficulty in avoiding endpoint effects and modal aliasing during signal decomposition [10,11]. VMD requires the number of decomposition layers and the penalty factor to be set in advance [12]. The difference in parameters will affect the diagnosis results.

Marine diesel engines are rotating machines. Their feature information often concerns the multiples of the rotational frequency. McFadden [13] proposed the time-domain synchronous averaging (TSA) method, which is essentially a series of equidistantly distributed bandpass filters. The

method is effective in suppressing noise interference but has some drawbacks. As a result, it is not widely used in the field of fault diagnosis. Relevant scholars have also suggested ways to improve it. Yin et al. [14] proposed an adaptive multiple TSA method, which solves the period selection problem. Ha et al. [15] used an autocorrelation TSA method to achieve fault diagnosis in wind turbines. Niaki et al. [16] combined VMD with TSA and successfully applied it to the fault diagnosis of the helical gearbox, solving the problem of diagnosing low-intensity faults. In [17], a moving interpolation method was used to optimise the TSA, which improves feature extraction under noisy conditions. In [18], the angular domain window synchronous averaging method was proposed, which overcame the waveform distortion caused by speed variations.

In summary, relevant scholars have improved TSA from different perspectives and successfully applied it in practical engineering. However, there are still certain problems:

(1) The TSA method tends to overlap specific frequency and frequency multiplication signal waveforms, making it difficult to decompose them effectively.
(2) After the signal has been averaged in the time domain, it is only possible to obtain feature information at a specific frequency; it is not possible to extract feature information in the full frequency domain at once.
(3) There is a need to acquire key phase signals. Although sensor technology is developing rapidly, the complex structure of marine diesel engines and the harsh operating environment makes it difficult to obtain key signals.

With advances in intelligence, deep learning methods have been extensively researched. The main methods are CNN, stacked auto-encoding networks, and deep belief networks [18-20]. In [21], a combination of continuous wavelet transforms (CWT) and CNN was used to achieve fault diagnosis of hydraulic piston pumps. Xu et al. [22] used ensemble empirical mode decomposition (EEMD) to decompose the vibration signal and then input its intrinsic modal functions into the CNN to achieve fault diagnosis of the bearing. Zhang et al. [23] obtained 2-D images by wavelet packet transformation of the original signals and input them into ResNet to achieve fault diagnosis of the gearbox. In [24], the signal-to-image conversion method was used to convert the original signals into two-dimensional images, which were then fed into the CNN for fault diagnosis of rotating machinery. Yan et al. [25] achieved fault diagnosis of a ship inverter by 1-D CNN. Li et al. [26] transformed the original signal into a two-dimensional image by using a signal-to-image conversion method and input it into a lightweight CNN, to realise the fault diagnosis of a marine centrifugal fan. Liu et al. [27] used the Gram angle field to transform the signal into a two-dimensional image and improve the residual network, to realise the fault diagnosis of rotor bearings. This shows that deep learning methods have made good progress in the field of fault diagnosis. Deep learning methods can overcome the inherent shortcomings of traditional intelligent fault diagnosis methods, such as the manual extraction of features and the difficulty of learning non-linear relationships.

Inspired by the above literature, a combination of a multi-scale time-domain averaging decomposition (MTAD) method, signal-to-image conversion and CNN is proposed for the fault diagnosis in marine diesel engines. The main contributions are as follows:

(1) The MTAD method can retain the feature information of the original signal more completely. The mutual interference of specific frequencies and frequency multiplication signals is overcome. There is no need to acquire key phase signals. The shortcomings of traditional TSA are overcome.
(2) The signal components are converted into 2-D images using signal-to-image conversion. This builds a bridge between computer vision and fault diagnosis.
(3) 2-D images are input into the CNN model for feature extraction and fault diagnosis. Fault diagnosis accuracy can be improved.

BASIC THEORY

TIME DOMAIN SYNCHRONOUS AVERAGING (TSA)

Given a vibration signal y(t) containing a periodic signal and other signals, the mean value of y(t) is zero. Assuming that it satisfies the Dirichlet condition, y(t) can be expressed as:

$$y(t) = g(t) + e(t) \tag{1}$$

where *g(t)* is a periodic signal and *e(t)* are other signals.

The period of the signal g(t) was T. The signal g(t) was divided into N segments of length T.. The nth segment sequence was defined as $P_n(\varphi)$. By the definition of the periodic function, it follows that:

$$P_n(\varphi) = P_{n+1}(\varphi) \tag{2}$$

where $n \in [1, N]$; phase $\varphi \in [0, T)$.

Partition *y(t)* into N time segments of equal length, with period T. $Y_n(\varphi)$ is the nth time segment and $Y_n(\varphi)$ can be expressed as:

$$Y_n(\varphi) = P_n(\varphi) + e_n(\varphi) \tag{3}$$

Since the mean value of y(t) is zero, $\sum_{n=1}^{N} e_n(\varphi) \approx 0$.

$$\sum_{\eta=1}^{N} Y_n(\varphi) \approx \sum_{\eta=1}^{N} P_n(\varphi) \tag{4}$$

Based on the above characteristics of *y(t)*, time-domain synchronous averaging can be expressed as the convolution of *y(t)* with the periodic signal *g(t)* [13]:

$$a(t) = (y * g)(t) = \frac{1}{N}\sum_{n=0}^{N-1} y(t + nT) \quad (5)$$

where $t \in [0, T)$ and *a(t)* is the TSA result for *y(t)*.

TSA extracts the fundamental and octave characteristics of rotating machinery and effectively suppresses noise interference. It is worth noting that the TSA is less resistant to interference when *N* is small. When analysing low-frequency signals, a longer time series is desirable, to prevent the *N* value from being too small and making it difficult to achieve the desired result.

The prerequisite for the above method is to obtain the key phase signals of the rotating machine. Depending on the characteristics of the comb filter, the relevant multiplier information can also be fused and difficult to decompose. In rotating machinery, signals from other periods may also contain fault information. TSA may also ignore other useful information when suppressing noise interference. Based on the above analysis, a multi-scale time-domain averaging decomposition method was proposed.

MULTI-SCALE TIME DOMAIN SYNCHRONOUS AVERAGING (MTAD)

The MTAD extracts the signal waveform at each frequency, aligns it with the original signal and decomposes it. This method can analyse the features of the signal at different frequencies and preserve the feature frequencies of the original signal more completely. In addition, it can suppress the coherence effects of frequency multiplication signals. It should be noted that the maximum frequency of the decomposition is determined by the type of fault. The maximum frequency should be greater than the frequency at which the fault is likely to exist. If the fault frequency cannot be determined, the highest frequency can generally be taken to be 0.5 times the sampling frequency. The calculation steps are as follows:

(1) The signal duration is *t*. $f_s = 0.5F_s - i \times s$, Time domain synchronous averaging of signals with period $T = \frac{1}{f_s}$. F_s is the sampling frequency. *s* is the step length. In general, $S = \frac{200}{tF_s}$. *i* is the number of iterations, $i < \frac{F_s}{2s}$.

(2) Dividing the original signal Y into K segments by period *T* can be expressed as:

$$Y = \bigcup_{k=1}^{k}\{y_k\} = \bigcup_{k=1}^{k}\{y_t\}, t \in [(k-1)T, kT) \quad (6)$$

Y is a discrete signal that can be interpolated with three times the spline at the corresponding coordinates of *y(t)*. $\boldsymbol{X}$ is the $\bigcup_{k=1}^{k}\{y_k\}$-based reconstruction matrix:

$$\boldsymbol{X} = \begin{bmatrix} y_1 \\ \cdot \\ \cdot \\ \cdot \\ y_K \end{bmatrix} = \begin{bmatrix} x_{11} \cdots x_{1n} \\ \cdot \\ \cdot \\ \cdot \\ x_{k_1} \cdots x_{kn} \end{bmatrix} \quad (7)$$

where n is the length of each periodic sequence, $n = \frac{T}{F_s}$.

If we assume that the mean of each column in the matrix $\boldsymbol{X}$ is , then the sequence of periods after averaging over the $\boldsymbol{X}$ time domain is $\bar{x} = [\bar{x}_1, \bar{x}_2 \ldots \bar{x}_n]$. $\overline{\boldsymbol{X}} = [\bar{x}, \bar{x} \ldots \bar{x}]$.

(1) The discrete sequence Y_{fs} can be obtained by a three times spline interpolation of $\overline{\boldsymbol{X}}$. The residual signal can be expressed as $Y_r = Y - Y_{fS}$.

(2) Increase the number of iterations and repeat steps (1) to (4) until the number of iterations exceeds the agreed condition.

(3) The time domain average decomposition result can be expressed as:

$$Y = Y_r + \Sigma Y_{fs} \quad (8)$$

During the decomposition process, a three-times spline interpolation of the signal is performed for each decomposition. This is due to the phase errors that accumulate when TSA processes discrete signals and can have an impact on the results. The MTAD uses the amplitude-frequency response feature to separate signals of different frequencies, avoiding the problem of mixing specific frequency signals and frequency multiplication signals in TSA. Each component represents the signal feature of the corresponding frequency. The feature containing the frequency band can be obtained by reconstructing the components of different frequency bands. For example, the reconstructed signal for frequency band $[f_{s1}, f_{s2}]$ is defined as:

$$Y' = \sum_{f_S=f_{S1}}^{f_{S2}} Yf_S \quad (9)$$

With MTAD, information can be extracted at different frequencies without a key phase signal, which is the basis for subsequent signal processing and fault diagnosis.

SIGNAL-TO-IMAGE CONVERSION

1-D signals can be converted into 2-D images by signal-to-image conversion [28]. The conversion process is shown in Fig. 1. If the obtained image size is $M \times M$, the length of the intercepted signal is M^2. The value of the signal is denoted by *L(i)*, i=1, …, M and the pixel size is denoted by *P (j, k)*, j=1, …, M, k=1, …, M. The formula can be expressed as:

$$P(j,k) = round\left\{\frac{L\big((j-1)\times M + k\big) - \mathrm{Min}(L)}{\mathrm{Max}(L) - \mathrm{Min}(L)} \times 255\right\} \quad (10)$$

where *round(.)* is the round function. Pixel values are normalised from 0 to 255. This method does not require any manual setting of the parameters and the features in the signal can be fully characterised.

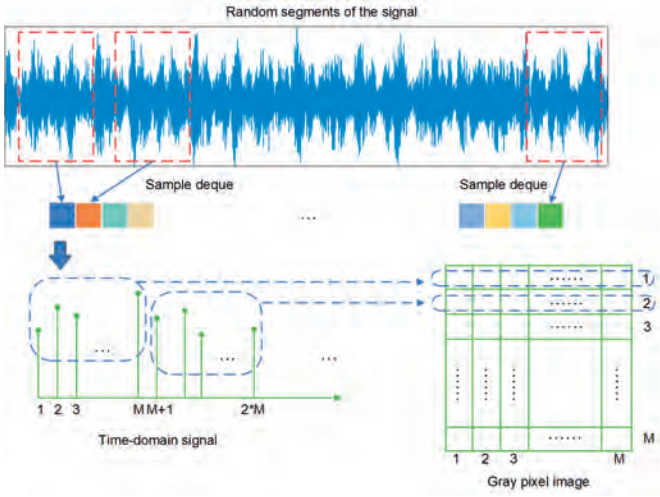

Fig. 1. The signal-to-image conversion process

EXPERIMENTAL ANALYSIS AND DISCUSSION

EXPERIMENTAL EQUIPMENT

The experimental diesel engine model was a MAN B&W 6S35ME-B. The rated power was 3250 kW and the rated speed was 142 r/min. The acceleration sensor model was INV9822, with a sampling frequency of 10.24 kHz. The data acquisition instrument was model INV3062 and the experimental platform is shown in Fig. 2. The marine diesel engine fault settings are given in Table 1. During the experiment, the diesel engine speed was 120 r/min and the power was 1800 kW.

Tab.1. Settings for different fault types

Fault label	Fault type	Fault setting	Training sample	Testing sample
1	Normal	-	500	300
2	No.1 cylinder misfire	Cut off No.1 cylinder fuel oil inlet valve	400	300
3	Cylinder knocking (Deflagration)	Reduce fuel oil viscosity (Rapid fuel oil changeover)	500	300
4	Inadequate air supply	Clogged air filter	400	300

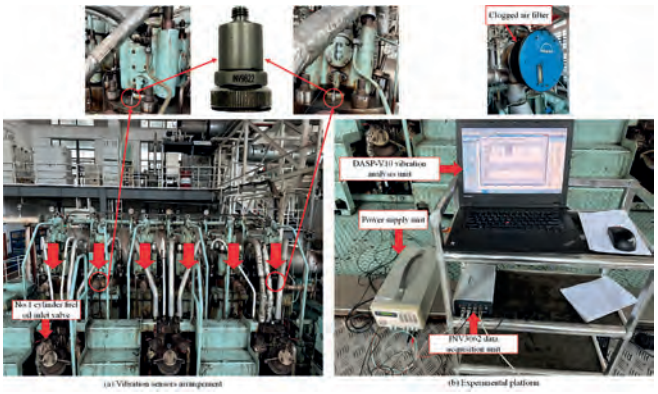

Fig. 2. Experimental platform

FAULT DIAGNOSIS PROCESS

The fault diagnosis flow chart is shown in Fig. 3. The main steps were as follows:

Step 1: Vibration signals of different health states were collected.

Step 2: The vibration signals were decomposed by MTAD and the time-frequency energy matrices obtained.

Step 3: 2-D images obtained by signal-to-image conversion and pseudo-colour coding. Training data was input into CNN and a CNN model was built to determine initial learning parameters.

Step 4: The testing data was input into a trained CNN model for feature extraction and fault diagnosis.

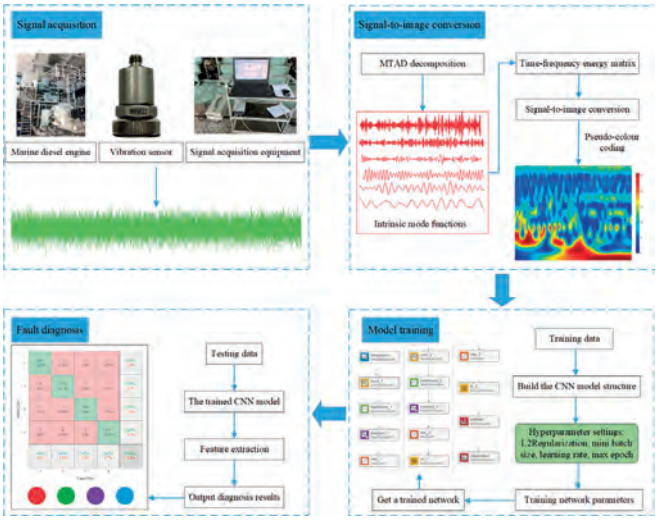

Fig. 3. Fault diagnosis flow chart

SIGNAL ANALYSIS

Normal condition and knocking cylinder failure are analysed as examples. The collected vibration signals were decomposed by MTAD at a step size of 0.5. The spectrum of the signal after MTAD decomposition is shown in Fig. 4. The intrinsic frequency of the diesel engine was 1.89 Hz and the signal cylinder firing frequency of the two-stroke diesel engine was equal to the rotation frequency (2.00 Hz). Under normal operating conditions, diesel engine vibration is mainly dominated by intrinsic frequency. When a cylinder knocking fault occurs, there is a significant change in vibration amplitude at both the intrinsic frequency and the six-fold frequency. The diesel engine was a six-cylinder diesel engine, so there was a significant change in amplitude at the six-fold frequency. The failure broke the dynamic balance of the engine. The amplitude also became prominent at the two and four-fold frequencies. The problem of waveform mixing between the intrinsic frequency and frequency multiplication signals was overcome by MTAD decomposition.

To link the computer vision and fault diagnosis, 1-D signals were transformed into 2-D images. In this way, invisible information from the original signal could be portrayed. The 1-D feature information was represented by textural features, such as colours and points of the 2-D image. Fig. 5 shows the results of the signal-to-image conversion for the four health states. When the cylinder knocking fault occurs, the time-frequency energy surges and has a certain time interval. For example, the energy intensity is higher at 0.0685 s, 0.2325 s, 0.3941 s, and 0.5592 s. The time interval is about 0.164 s. A lower energy component exists between each of the two higher energies, i.e. the energy intensity changes every 0.082 s. During this period, the frequency is approximately 12.19 Hz, which is very close to the frequency of a cylinder knocking failure (12.27 Hz).

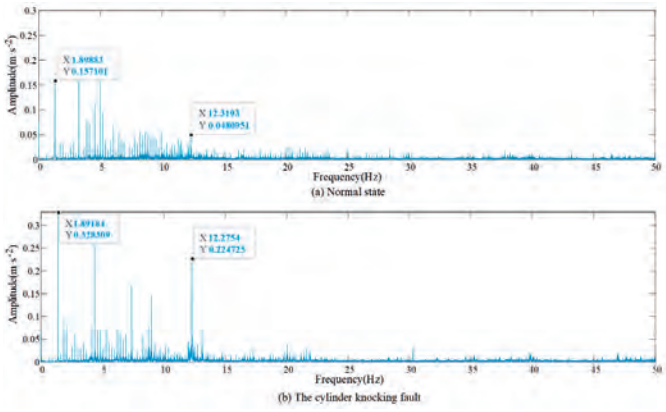

Fig. 4. Spectrogram after MTAD decomposition

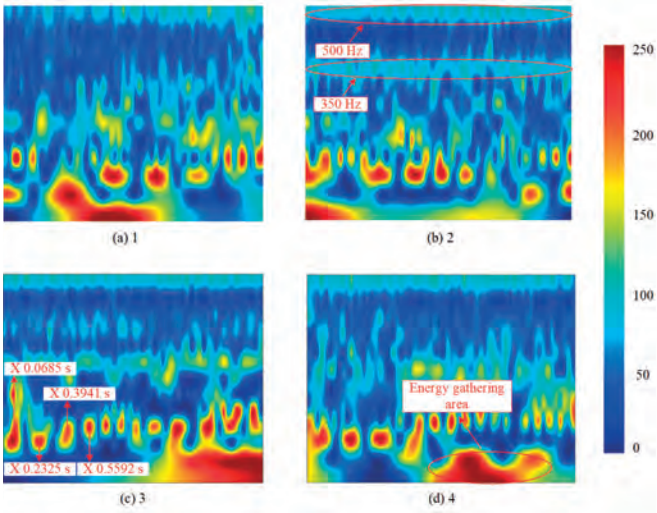

Fig. 5. Signal-to-image conversion results for four different health states

CNN MODEL

The CNN model required some hyperparameters to be set before it could be trained and tested. MaxEpoch and Learning rate were used as an example, to demonstrate the hyperparameter determination process. The optional values of MaxEpoch were set as 20, 30, 40, 50, and 80. The optional values of the learning rate was 0.0001, 0.001, and 0.01. The optional value of mini batch size was 50, 75, 100, and 125. The effect of different hyperparameters on the network performance is shown in Figs 6, 7 and 8, respectively. When MaxEpoch = 20, the network model was less time-consuming and had high diagnostic accuracy. Therefore, MaxEpoch was set the value of 20. The network performance is optimal when the learning rate is 0.001. The network performs best when the mini batch size is 50. Other hyperparameters were set in a similar way and the finally determined hyperparameters are shown in Table 2. The CNN model used in this paper had 17 layers, structured as shown in Fig. 9. The specific network model parameters are presented in Table 3.

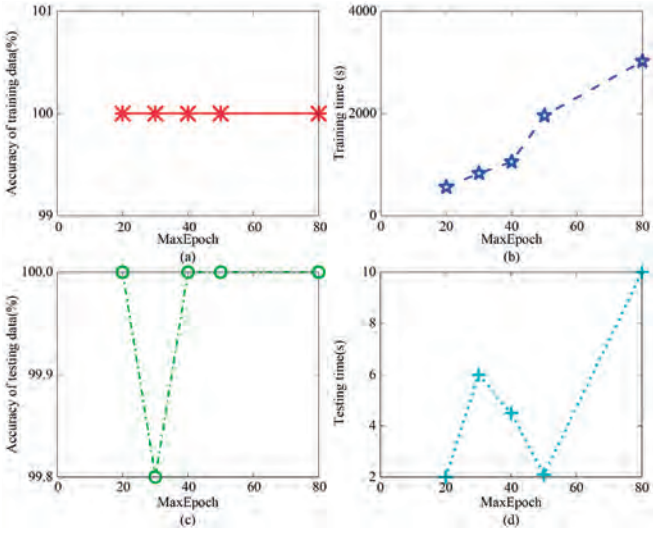

Fig. 6. Experimental results for different values of MaxEpoch

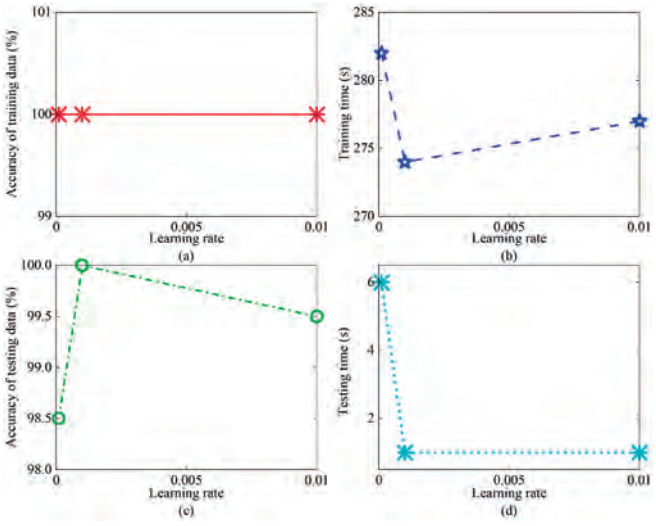

Fig. 7. Experimental results for different learning rates

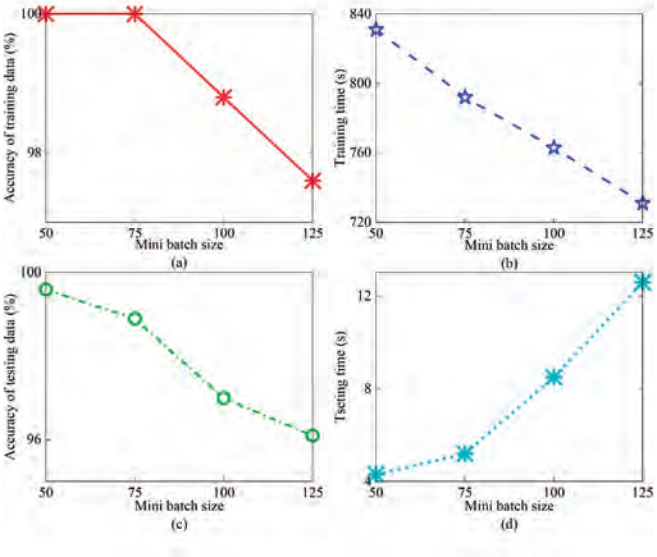

Fig. 8. Experimental results for different mini batch sizes

Tab. 2. Results of initial learning parameter settings

LearnRate	0.001
LearnRateDropFactor	0.05
LearnRateDropPeriod	10
L2Regularisation	0.004
MaxEpoch	20
MiniBatchSize	50
Solver	Adam

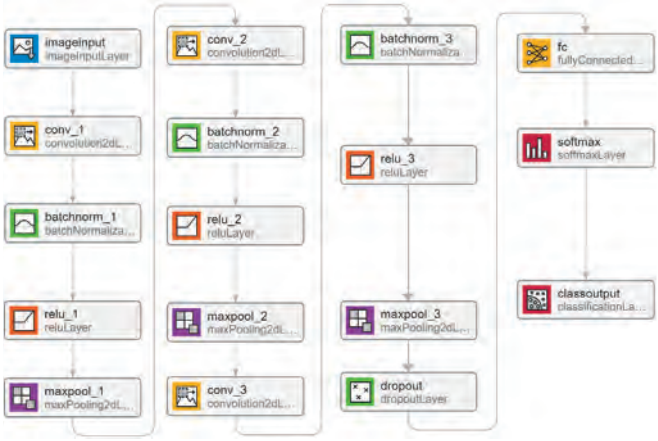

Fig. 9. The CNN model structure diagram

Tab. 3. The CNN structural parameters

Name	Activations	Learnables
imageinput	120×120×3	-
conv_1	120×120×16	Weights 6×6×3×16 Bias 1×1×16
batchnorm_1	120×120×16	Offset 1×1×16 Scale 1×1×16
relu_1	120×120×16	-
maxpool_1	60×60×16	-
conv_2	60×60×32	Weights 4×4×16×32 Bias 1×1×32
batchnorm_2	60×60×32	Offset 1×1×32 Scale 1×1×32
relu_2	60×60×32	-
maxpool_2	30×30×32	-
conv_3	30×30×64	Weights 4×4×16×64 Bias 1×1×64
batchnorm_3	30×30×64	Offset 1×1×64 Scale 1×1×64
relu_3	30×30×64	-
maxpool_3	15×15×64	-
dropout	15×15×64	-
fc	1×1×4	Weights 4×14 Bias 4×1
softmax	1×1×4	-
classoutput	-	-

FAULT DIAGNOSIS

The operating environment was Windows 11 and the software environment comprised Anaconda 3, Python 3.9.13 and MATLAB 2021a. The deep learning framework was PyTorch 1.11.0. After pre-training the model with training data, the test data was input into the model for fault diagnosis. The network training process and testing process are shown in Fig. 10. The number of iterations in each round was 98, with a total of 20 iterations, and the maximum number of iterations was 1960. According to Fig. 10(a), as the number of iterations increased, the accuracy of the training data increased until it reached 100%. At the same time, the accuracy rate of the test data also increased and gradually approached 100%.

According to Fig. 10(b), the loss function values for both the training and test data gradually decreased until they levelled off. The final value of the loss function for the training data was 0.039. The final value of the loss function for the test data was 0.085. The training time was 251 s and the testing time was 36 s. The CNN model had a superior response speed and no over-fitting of the model occurred during the diagnosis.

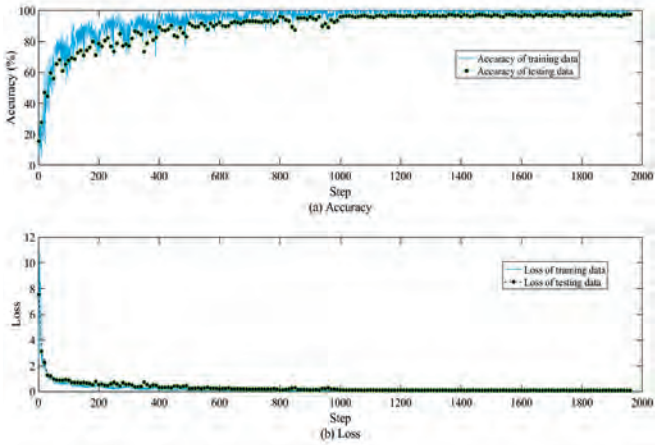

Fig. 10. The CNN model training and testing process

In order to validate the CNN model's capability for feature extraction, the clustering effect was visualised and analysed at different stages. The feature distribution of the network structure is analyzed by T-SNE visualization [29]. It can map high-dimensional data to 2-D space well and the visualisation results of different layers are shown in Fig. 11. Different feature information is mixed in the input layer. After two levels of convolution, the same feature information tends to be clustered and different feature information is distributed in different regions. In the softmax layer, the different feature information was completely separated. The network model was very effective in classifying four different health states.

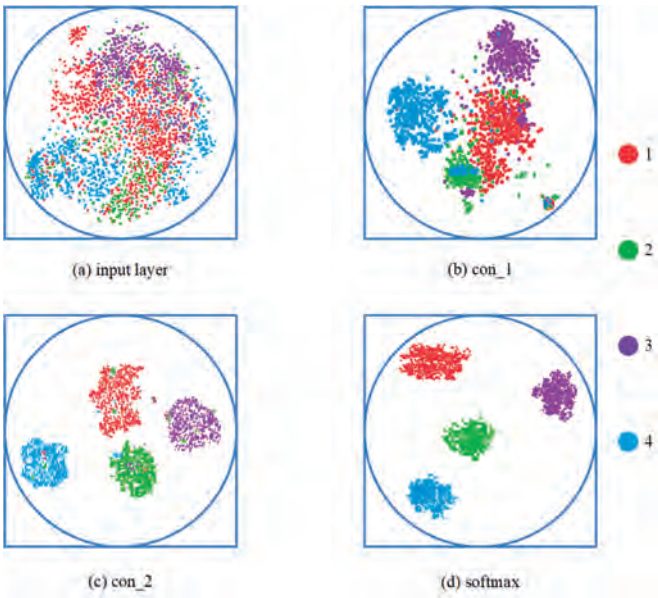

Fig. 11. Results of feature visualisation for different layers

COMPARATIVE ANALYSIS OF DIFFERENT METHODS

The comparative analysis methods used in the experiments were EEMD-CNN [22], MVMD-CNN [12], CWT-CNN [21], and ResNet [23]. In MVMD-CNN, the number of VMD decomposition layers is determined adaptively, using the partial mean of the multi-scale permutation entropy. It can effectively overcome mode aliasing. In CWT-CNN, the original signals are transformed into 2-D images by continuous wavelet transform, which has good time-frequency aggregation. In ResNet, the introduction of residual connectivity enables the extraction of deep feature information while preserving shallow feature information. Different diagnostic methods are analysed in the case of different signal-to-noise ratios (SNR). The diagnostic accuracy of the above methods, at different SNR(s), is shown in Fig. 12.

Fig. 12 shows that, as the noise intensity increased (SNR decreased), the accuracy of the different methods decreased. When SNR = -5 dB, the proposed method achieved a diagnostic accuracy of 94.5%, which is 3.8~8.7% higher than with other methods. When SNR = 30 dB, the confusion matrix of the testing data is shown in Fig. 13. A total of 15 test samples are misclassified. The diagnostic accuracy for the four health states is 99.0%, 99.0%, 98.7% and 98.3%, respectively. The average diagnostic accuracy is 98.8%. In summary, the proposed method is effective in extracting feature information from the original signal and has a certain anti-noise capability.

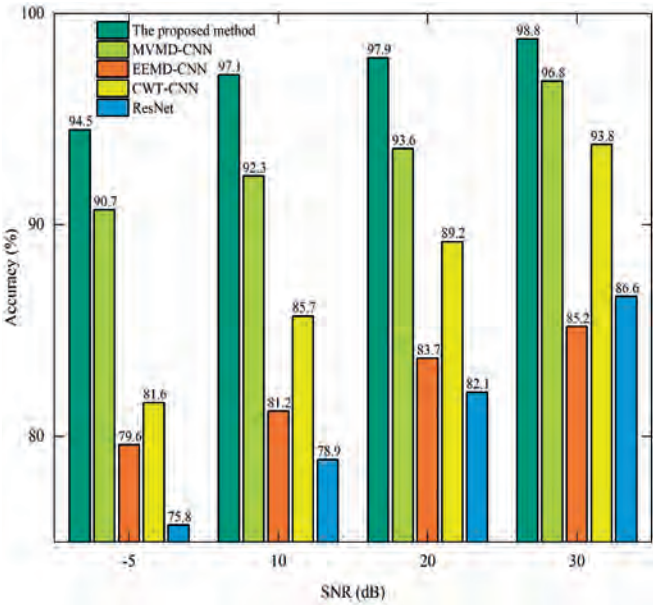

Fig. 12. Comparison of the diagnostic accuracy of different methods

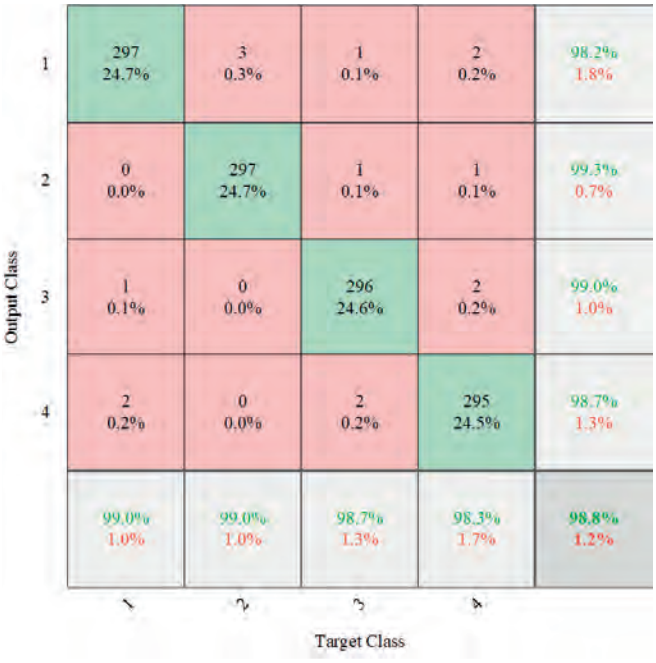

Fig. 13. Confusion matrix for testing data (SNR = 30 dB)

CONCLUSIONS

In this work, a fault diagnosis method for a marine diesel engine is proposed and validated, based on multi-scale time-domain averaging decomposition, signal-to-image conversion and CNN. The conclusions are as follows:

(1) MTAD can effectively separate frequency multiplication signals. There is no loss of feature information and there is no need to obtain key phase signals. The effectiveness of MTAD is verified by the experiments. MTAD overcomes the limitations of traditional methods.

(2) The signal-to-image conversion method can portray the invisible information of the raw signals. The textural features of the 2-D images can make the differences in signal features between working conditions more apparent.

(3) The accuracy of the proposed method is stable: above 94.0% at different SNR(s). When SNR = -5 dB, the accuracy of the proposed method is 3.818.7% higher than other methods. It has a certain level of adaptive noise immunity.

Due to the limitations of the experimental conditions, only a few typical faults of diesel engines are preset in the experiments. In the next step, a more comprehensive study should be carried out for each subsystem of the diesel engine.

REFERENCES

1. [1] Shi QG, Hu YH, Yan GH. Hierarchical multiscale fluctuation dispersion entropy for fuel injection system fault diagnosis. Polish Maritime Research, vol. 30, no. 1, pp. 98-111, 2023, https://doi.org/10.2478/pomr-2023-0010.

2. [2] Gültekin Ö, Çinar E, Özkan K, Yazıcı A. A novel deep learning approach for intelligent fault diagnosis applications based on time-frequency images. Neural Computing and Applications, vol. 34, no. 6, pp. 4803-4812, 2022, https://doi.org/10.1007/S00521-021-06668-2.

3. [3] Anwarsha A, Narendiranath B. A review on the role of tunable Q-Factor wavelet transform in fault diagnosis of rolling element bearings. Journal of Vibration Engineering & Technologies, vol.10, no. 5, pp. 1793-1808, 2022, https://doi.org/10.1007/S42417-022-00484-1.

4. [4] He L, Liu Q, Jiang Z. Combined underdamped bistatic stochastic resonance for weak signal detection and fault diagnosis under wavelet transform. Fluctuation and Noise Letters, vol. 22, no. 1, pp. 2350007, 2023, https://doi.org/10.1142/S0219477523500074.

5. [5] Cheng Y, Lin M, Wu J, Zhu H, Shao X. Intelligent fault diagnosis of rotating machinery based on continuous wavelet transform-local binary convolutional neural network. Knowledge-Based Systems, vol. 216, pp. 106796, 2021, https://doi.org/10.1016/J.KNOSYS.2021.106796.

6. [6] Shafiullah M, AlShumayri KA, Alam MS. Machine learning tools for active distribution grid fault diagnosis. Advances in Engineering Software, vol. 173, pp. 103279, 2022, https://doi.org/10.1016/J.ADVENGSOFT.2022.103279.

7. [7] Zhou X, Wang X, Wang H, Cao L, Xing Z, Yang Z. Rotor fault diagnosis method based on VMD symmetrical polar image and fuzzy neural network. Applied Sciences, vol. 13, no. 2, pp. 1134, 2023, https://doi.org/10.3390/APP13021134.

8. [8] Mohammed EAK, Ameur FA, Ahmed HB, Noureddine B, Azeddine B. Bearing fault diagnosis of a PWM inverter fed-Induction motor using an improved short time Fourier transform. Journal of Electrical Engineering & Technology, vol. 14, no. 3, pp. 1201-1210, 2019, https://doi.org/10.1007/s42835-019-00096-y

9. [9] Hou SZ, Guo W, Wang Z, Liu Y. Deep-learning-based fault type identification using modified CEEMDAN and image augmentation in distribution power grid. IEEE Sensors Journal, vol. 22, no. 2, pp. 1583-1596, 2022, https://doi.org/10.1109/JSEN.2021.3133352.

10. [10] Liu Z, Peng D, Zuo M, Xia J, Qin Y. Improved Hilbert-Huang transform with soft sifting stopping criterion and its application to fault diagnosis of wheelset bearings. ISA transactions, vol. 125, pp. 426-444, 2021, https://doi.org/10.1016/J.ISATRA.2021.07.011.

11. [11] Ji Y, Wang H. A revised Hilbert-Huang transform and its application to fault diagnosis in a rotor. System Sensors (Basel, Switzerland), vol. 18, no. 12, pp. 4329, 2018, https://doi.org/10.3390/s18124329.

12. [12] Hou SZ, Guo W. Fault identification method for distribution network based on parameter optimized variational mode decomposition and convolutional neural network. IET Generation, Transmission & Distribution, vol. 16, no. 4, pp. 737-749, 2021, https://doi.org/10.1049/GTD2.12324.

13. [13] McFadden PD. A revised model for the extraction of periodic waveforms by time domain averaging. Mechanical Systems and Signal Processing, vol. 1, no. 1, pp. 83-95, 1987, https://doi.org/10.1016/0888-3270(87)90085-9.

14. [12] Yin N, Meng Z, Guan Y, Fan F. An adaptive multiple time domain synchronous averaging method and its application in vibration signal feature enhancement. Measurement Science and Technology, vol. 33, no. 5, pp. 055004, 2022, https://doi.org/10.1088/1361-6501/AC3D08.

15. [15] Jong MH, Byeng DY, Hyunseok O, Bongtae H, Yoongho J, Jungho P. Autocorrelation-based time synchronous averaging for condition monitoring of planetary gearboxes in wind turbines. Mechanical Systems and Signal Processing, vol. 70, pp. 161-175, 2016, https://doi.org/10.1016/j.ymssp.2015.09.040.

16. [16] Tofighi NS, Alavi H, Ohadi A. Incipient fault detection of helical gearbox based on variational mode decomposition and time synchronous averaging. Structural Health Monitoring, vol. 22, no. 2, pp. 1494-1512, 2023, https://doi.org/10.1177/14759217221108489.

17. [17] Huang ZF, Sun KC, Wei DH, Mao HL, Li XX, Qian X. Improved time domain synchronous averaging based on the moving interpolation and kurtosis criterion searching. Measurement Science and Technology, vol. 32, no. 10, pp. 105010, 2021, https://doi:10.1088/1361-6501/AC02F6.

18. [18] Xu ZF, Zhang CC, Liu SH, Zhang W, Zhang YF. Research on fault diagnosis of rolling bearings in roller-to-roller printing units based on Siamese network. Journal of Low Frequency Noise, Vibration and Active Control, vol. 42, no. 1, pp. 403-419, 2023, https://doi.org/10.1177/14613484221119897.

19. [19] Liu BW, Chai Y, Jiang YT, Wang YM. Industrial fault detection based on discriminant enhanced stacking auto-encoder model. Electronics, vol. 11, no. 23, pp. 3993, 2022, https://doi.org/10.3390/ELECTRONICS11233993.

20. [20] Tang JH, Wu JM, Hu BB, Liu J. Towards a fault diagnosis method for rolling bearing with Bi-directional deep belief network. Applied Acoustics, vol. 192, 2022, https://doi.org/10.1016/J.APACOUST.2022.108727.

21. [21] Tang SN, Zhu Y, Yuan SQ. An adaptive deep learning model towards fault diagnosis of hydraulic piston pump using pressure signal. Engineering Failure Analysis, vol. 138, 2022, https://doi.org/10.1016/J.ENGFAILANAL.2022.106300.

22. [22] Xu ZB, Wang Y, Xiong W, Wang ZG. A novel attentional feature fusion with inception based on capsule network and application to the fault diagnosis of bearing with small data samples. Machines, vol. 10, no. 9, pp. 789, 2022, https://doi.org/10.3390/MACHINES10090789.

23. [23] Zhang K, Tang BQ, Deng L, Liu XL. A hybrid attention improved ResNet based fault diagnosis method of wind turbines gearbox. Measurement, vol. 179, 2021, https://doi.org/10.1016/J.MEASUREMENT.2021.109491.

24. [24] Wang HQ, Li S, Song LY, Cui LL. A novel convolutional neural network based fault recognition method via image fusion of multi-vibration-signals. Computers in Industry, vol. 105 pp. 182-190, 2019, https://doi.org/10.1016/j.compind.2018.12.013.

25. [25] G. H. Yan, Y. H. Hu, Q. G. Shi, "A convolutional neural network-based method of inverter fault diagnosis in a ship's DC electrical system," Polish Maritime Research, vol. 29, no. 4, pp. 105-114, 2022, https://doi.org/10.2478/pomr-2022-0048.

26. [26] Li CY, Hu YH, Jiang JW, Yan GH. Deep learning-based fault diagnosis for marine centrifugal fan. Polish Maritime Research, vol. 30, no. 1, pp.112-120, 2022, https://doi.org/10.2478/pomr-2023-0011.

27. [27] Liu FY, Li WJ, Wu YZ, He YH, Li TY. Fault diagnosis of imbalance and misalignment in rotor-bearing systems using deep learning. Polish Maritime Research, vol. 31, no. 1, pp. 102-113, 2024, https://doi.org/10.2478/pomr-2024-0011.

28. [28] Wen L, Li XY, Gao L, Zhang YY. A new convolutional neural network-based data-driven fault diagnosis method. IEEE Transactions on Industrial Electronics, vol. 65, no.7, pp. 5990-5998, 2018, https://doi.org/10.1109/tie.2017.2774777.

29. [29] Cui YB, Wang RJ, Si YP, et al. T-type inverter fault diagnosis based on GASF and improved AlexNet. Energy Reports, vol. 9, pp. 2718-2731, 2023, https://doi.org/10.1016/J.EGYR.2023.01.095.